A Case Study of Aerosol Data Assimilation with the Community Multi-Scale Air Quality Model over the Contiguous United States using 3D-Var and Optimal Interpolation Methods

Youhua Tang[1,2] (youhua.tang@noaa.gov), Mariusz Pagowski[4,5], Tianfeng Chai[1,2], Li Pan[1,2], Pius Lee[1], Barry Baker[1,2], Rajesh Kumar[6], Luca Delle Monache[6], Daniel Tong[1,2,3], and Hyun-Cheol Kim[1,2]

1. NOAA Air Resources Laboratory, College Park, MD.
2. Cooperative Institute for Climate and Satellites, University of Maryland at College Park, MD.
3. Center for Spatial Information Science and Systems, George Mason University, Fairfax, VA.
4. NOAA Earth System Research Laboratory, Boulder, CO.
5. Cooperative Institute for Research in Environmental Sciences, University of Colorado, Boulder, CO.
6. National Center for Atmospheric Research, Boulder, CO.

Abstract

This study applies the Gridpoint Statistical Interpolation (GSI) 3D-Var assimilation tool originally developed by the National Centers for Environmental Prediction (NCEP), to improve surface $PM_{2.5}$ predictions over the contiguous United States (CONUS) by assimilating aerosol optical depth (AOD) and surface $PM_{2.5}$ in version 5.1 of the Community Multi-scale Air Quality (CMAQ) modeling system. An optimal interpolation (OI) method implemented earlier (Tang et al., 2015) for the CMAQ modeling system is also tested for the same period (July, 2011) over the same contiguous United States (CONUS). Both GSI and OI methods assimilate surface $PM_{2.5}$ observations at 00, 06, 12, and 18UTC, and MODIS AOD at 18 UTC. The assimilations of observations using both GSI and OI generally help reduce the prediction biases, and improve correlation between model predictions and observations. In the GSI experiments, assimilation of surface $PM_{2.5}$ leads to stronger increments in surface $PM_{2.5}$ compared to its MODIS AOD assimilation at the 550nm wavelength. In contrast, we find a stronger OI impact of the MODIS AOD on surface aerosols at 18 UTC compared to the surface $PM_{2.5}$ OI method. GSI produces smoother result and yields overall better correlation coefficient and root mean squared error (RMSE). It should be noted that the 3D-var and OI methods used here have several big difference besides the data assimilation schemes. For instance, the OI uses the relatively big model uncertainties, which helps yield smaller mean biases, but sometimes causes the RMSE increase. We also examine and discuss the sensitivity of the assimilation experiments results to the AOD forward operators.

1. Introduction

The existing U.S. National Air Quality Forecasting Capability (NAQFC) run by the National Oceanic and Atmospheric Administration (NOAA)/National Centers for Environmental Prediction (NCEP) provides daily 48-hour ozone and $PM_{2.5}$ (particle matters with diameter < 2.5 μm) forecasts using the Community Multi-scale Air Quality (CMAQ) modeling system with 12km horizontal grid resolution. Many contributions toward improving the NAQFC can be found in literatures, including updated emission, meteorology, chemical mechanism and lateral boundary conditions (Pan et al., 2014; Tang et al., 2008; Lee et al., 2016). However, biases still contaminate current predictions.

Chemical data assimilation techniques have been developed to improve initial conditions of chemical transport models (CTM) and yield better prediction ((Elbern et al., 1997, 2000, 2007; Elbern and Schmidt, 1999, 2001; Bocquet et al., 2015) by blending the information from a model estimate (refer to as prior or background) and from observations in certain methods. One method is direct blending, e.g. using observed chemical mass concentrations to correct the modeled mass concentrations, which is relatively straightforward, as they are directly comparable. As most monitoring data are located near surface, that method was usually applied to near-surface field. Another method is indirect guessing, e.g. comparing satellite retrieved AOD with modeled AOD to estimate the biases of modeled column mass concentrations and make the corresponding adjustment. Tang et al. (2015) used both surface $PM_{2.5}$ and MODIS AOD to adjust the initial condition of a CTM with the optimal interpolation (OI) method, and successfully reduced the model biases. The OI correction was applied to 7×7 or 11×11 grid cells horizontally, and from the ground to the boundary layer top vertically for surface $PM_{2.5}$ assimilation. Adhikary et al. (2008) and Chai et al. (2017) also used the similar local OI correction to reduce model biases. A more complex method is using the Gridpoint Statistical Interpolation (GSI) (Wu et al., 2002; Purser et al., 2003a, b), a 3D-VAR method, developed by NOAA/NCEP. It has been applied to assimilate the Goddard Chemistry Aerosol Radiation and Transport (GOCART) aerosols in Weather Research and Forecasting model coupled with Chemistry (WRF-CHEM) with its 3D-var method (Pagowski et al., 2014; Liu et al., 2011). In next sections, we describe the method that extends the GSI to assimilate CMAQ aerosols comparing to the OI correction. A comparison for their one-month performances will be discussed.

2. Methodology and Settings

The baseline model setting used in this study is similar to Tang et al. (2015), except that the CMAQ model changed from version 5.0.2 to version 5.1 for more refined chemical mechanisms and physical schemes. The meteorology is provided by the WRF-ARW (version 3.4.1) driven by the NCEP FNL (Final Global Analysis) 1° × 1° analysis field and was reinitialized every 24 hour. Both the meteorological and air quality models have 12-km horizontal resolution over the

contiguous United States, with 42 sigma layers vertically, and the domain tops at 50 hPa. The detailed setting of the CMAQ model can be found in Tang et al. (2015). Chai et al (2017) described the detail of the OI algorithm for aerosol assimilation, and that study used relatively old CMAQ (version 4.7.1) with 22 vertical layers. In order to compare the two methods of adjusting the initial condition, we assimilate same surface $PM_{2.5}$ data, the USEPA Air Quality System (AQS) data, 4 times every day (00Z, 06Z, 12Z and 18Z). The 18Z assimilation uses additional MODIS AOD data from Terra and Aqua satellites, whose overpassing time over the CONUS domain range from 14 to 22 UTC, depending on the dates and locations. In this study, we only used the MODIS AOD at 550 nm wavelength (Level-2 MODIS AOD from the Collection 051 with the best quality, quality flag = 3) (Levy et al., 2009).

2.1 Settings for Data Assimilations

In this study, we are comparing two assimilation methods: the optimal interpolation and GSI's 3D-Var. The optimal interpolation is carried in the similar way as described in the OI4 case of Tang et al. (2015) for assimilating surface $PM_{2.5}$ and aerosol optical depth retrieved from Aqua/Terra MODIS sensors at 550nm.

$$X^a = X^b + BH^T(HBH^T + O)^{-1}(Y - HX^b) \quad (1)$$

where X^a and X^b are the analyzed and background (prior modeled) concentrations or aerosol optical depth (AOD) data, B and O are the background and observation error covariance matrices, H is the observational operator and H^T is its matrix transpose, and Y is the observation vector. The relative uncertainty setting is also same as Tang et al. (2015), in which the background relative uncertainties have horizontal and diurnal variations. Before the OI assimilation, the AQS surface $PM_{2.5}$ monitoring data and MODIS AOD data are put into their corresponding model grids. If there was more than one active surface $PM_{2.5}$ station in the same model grid, the observation was taken from their average. The OI adjustment is made on each 11×11 grid cells horizontally throughout the whole domain, and gets the analyzed field X^a. Then the ratio of X^a/X^b at each grid point is used to scale all aerosol components throughout the vertical column. The surface $PM_{2.5}$ OI is applied from surface to the height of the planetary boundary layer (PBL), and the MODIS AOD is used to adjust above-PBL aerosol after deducting the adjusted below-PBL AOD.

The GSI's 3D-var uses a similar approach (Pagowski et al., 2014; Liu et al., 2011) for its cost function

$$J = \frac{1}{2}(x_a - x_b)^T B^{-1}(x_a - x_b) + \frac{1}{2}(Hx_a - O_o)^T O^{-1}(Hx_a - O_o) + Jc \quad (2)$$

Where x_a and x_b are the analyzed and background (a prior modeled) concentrations or AOD data, B and O are the background and observation error covariance matrices, H is the observational operator, O_o is the observations and J_c is the constraint terms. Both GSI's 3D-Var and OI use spatially varied background bias and observation to make the adjustment. However, each OI adjustment used in this study is made in each 11×11 grid horizontally and its effect expands up to the PBL height for its surface $PM_{2.5}$ assimilation. The GSI's cost function reduction is performed for the whole domain, and its effect of the adjustment can be expanded in much greater horizontal and vertical scales defined by its horizontal and vertical length scales, respectively.

In this study, we carry out the similar uncertain setting for the OI as Tang et al. (2015), in which the background's relative uncertainties have horizontal and diurnal variations (Figure 2 of Tang et al., 2015) for PM2.5 assimilation over the $PM_{2.5}$ monitoring locations, and a fixed relative uncertainty of 80% are applied to the other areas.. In the OI horizontal adjustment, its B matrix has cut-off Gaussian-like horizontal correlations for its each 11×11 grid adjustment. For OI's AOD assimilation, we use the fixed relative uncertainty of 80% for modeled AOD. MODIS AOD's retrieval quality depends on the land surface properties, and its uncertainty can be range from 5% over ocean to 20% over land (Remer et al., 2005). Although the surface in-situ measured AQS $PM_{2.5}$ has much less measurement error than the satellite-retrieved AOD in most scenarios, the single surface station's representative error over the 12km grid cell could be higher than the MODIS AOD which is in 10×10km resolution. In this study, we simply choose the relatively uncertainty of 10% for both MODIS AOD and surface $PM_{2.5}$ observations. In this study, the PM2.5 observations are located at 674 surface sites over CONUS, and all of them are used in data assimilations.

GSI's setting is similar to Pagowski et al. (2014), in which the background error and length scales have vertical variance. Figure 1 shows that the vertical profiles of background errors and length scales for $PM_{2.5}$ (for $PM_{2.5}$ assimilation) and accumulation-mode sulfate (ASO4J, for AOD assimilation), which can be calculated using GSI's NMC (National Meteorological Center) method (Parrish and Derber, 1992) with a tool called GEN_BE (Descombes et al., 2015). ASO4J is one of CMAQ aerosol species used in AOD data assimilation. Other aerosol species have similar model or background errors. The uncertainties of modeled aerosols are high in the lower layers and decrease with altitudes. The model's horizontal length scale indicates the extent of the assimilation's horizontal expansion. In Figure 1, the horizontal length scale for modeled $PM_{2.5}$ increases significantly around the altitude of 12km, where the tropopause is usually located. The model's vertical length scale indicates the extent of the assimilation's vertical expansion, which is related to the strength of vertical advection, diffusion, and convection. Below PBL, the vertical length scale is usually stronger than that in the upper layers. GSI was mainly used for assimilating meteorological variables, such as temperature and humidity, which usually have strong latitude variation. So, the vertical profiles of background errors and length scales used in GSI for meteorological variables were usually varied depending on latitudes. In this study, our

assimilation target are aerosols, whose concentrations and the corresponding variance could be caused by many factors, including emission, transport and chemical transformation, and their latitude dependences are not significant. So, we simply use one set of the vertical profiles for each aerosol species throughout the whole domain, which has no temporal variation, either. We use the same constant observation error of 0.1 in GSI for surface $PM_{2.5}$ and MODIS AOD. In both settings of GSI and OI, their background errors are far greater than the observation errors in lower altitudes, which push the adjusted values toward the observed surface $PM_{2.5}$. For AOD assimilations, GSI's main increment is also in low altitudes due to its background error profile (Figure 1), while OI's AOD assimilation applies one adjusting ratio to whole column for each grid cell.

2.2 Calculations of Aerosol Optical Depths

To assimilate AOD in the CMAQ model, we need convert CMAQ aerosol chemical compositions. CMAQ includes two methods for calculating AOD: the Mie method and the reconstruction method (Binkowski and Roselle, 2003). The Mie method calculates the aerosol optical extinction coefficient (AOE) from modeled aerosol physical characteristics, including the index of refraction, volume concentration and aerosol size distributions. It does not require aerosol chemical composition information and can handle the aerosols' internal mixture, in which each aerosol particle is composed of a solid core and coating layers of various compositions due to the aerosol uptake. In theory, the Mie method should yield accurate AOE if all the model's aerosol physical properties are correct. However, that condition was hard to reach in many circumstances. Also, aerosol mass concentrations are often available in both models and observations, and a convenient method is needed to directly convert aerosol mass concentrations to AOE. So, CMAQ provides another empirical approach, the reconstruction method (RM), which uses the mass concentrations of aerosol chemical compositions to calculate the total AOE with a look-up table. The RM assumes that all aerosols are externally mixed. It calculates each composition's AOE, and sums them up to get the total AOE (Binkowski and Roselle, 2003) for the wavelength at 550nm.

$$AOE\left[\frac{1}{km}\right] = 0.003 * f(RH) * \{(NH_4)_2SO_4 + NH_4NO_3\} + 0.004 * \{oragnic\ mass\} + 0.01 * \{light\ absorbing\ carbon\} + 0.001 * \{fine\ soil\} + 0.0006 * \{coarse\ mass\} + 0.00137 * f_s(RH) * \{sea\ salt\} \quad (3)$$

In CMAQ's RM, only the AOE from ammonium, sulfate, nitrate, and sea salt have the dependence on relative humidity (RH). *f(RH)* and $f_s(RH)$ are two RH-dependent look-up tables of aerosol hydroscopic growth for sulfate/nitrate/ammonium and sea salt, respectively (the original RM (Binkowski and Roselle, 2003) in earlier versions (<5.1) of CMAQ does not include sea salt's RH dependence for AOE calculation). All other aerosols are converted from their mass concentrations to the corresponding AOEs with simple fixed constants. The conversion method does not need aerosol size distribution, but just the mass concentrations of aerosol compositions

and ambient RH. Due to its simplicity and convenience, the RM method is widely used not only for CMAQ aerosols, but also for converting observed aerosol mass concentrations to AOE (Malm et al., 1994; Roy et al., 2007). Tang et al. (2015) also use the RM calculated AOD for OI assimilation, which is carried out here for this OI assimilation. In contrast, the Mie method based on aerosol physical characteristics is relatively hard to be used in data assimilations, as the data assimilations target the mass concentrations of aerosol compositions, not the aerosol physical characteristics directly. Although we can use adjusted aerosol mass concentrations to calculate the corresponding change on aerosol physical characteristics with CMAQ routines, and then link it to AOD adjustment, the additional conversion makes these calculations difficult.

In theory, we should use the same forward method, such as RM, to calculate AOD used in GSI. However, the CMAQ's current RM is relatively simple, only for single wavelength, 500nm, without considering aerosol distribution. The current RM can not be directly used to calculate multi-wavelength AOD, though this study only uses the 550nm AOD. The existing GSI has its own tool, the Community Radiative Transfer Model (CRTM, Han et al., 2006; Liu and Weng, 2006), to handle its AOD calculation. CRTM provides GSI not only the forward AOD, but also the calculations of tangent-linear, adjoint and K-matrix for multiple wavelengths. As the GSI is tightly coupled with CRTM for its AOD related operations, we need to go through the CRTM for utilizing GSI's existing AOD assimilation capability. However, the current version of CRTM does not support CMAQ's aerosol species, and only handle GOCART (Goddard Chemistry Aerosol Radiation and Transport, Chin et al., 2000, 2002) aerosol species. GOCART's aerosol species are similar to the classification of aerosol used in CMAQ RM method, including sulfate, dust, sea salt, black carbon, and organic carbon, which also assumes that the aerosols are externally mixed. It is possible for us to represent CMAQ aerosols in GOCART aerosol categories for calculating their optical properties. Table 1 shows how the CMAQ 5.1 Aero6 species (Sonntag et al., 2014) are mapped to CRTM's GOCART aerosol. CMAQ aerosols have 3 size modes: Aitken (i-mode), accumulation (j-mode) and coarse mode (k-mode) representing the super-fine nucleation particles, aged coagulated particles, and coarse particles, respectively (Binkowski and Roselle, 2003). Each size mode has its own lognormal size distribution (Whitby and McMurry, 1997).We applied the CMAQ averaged aerosol size for each mode (aitken, accumulation or coarse) to the CRTM AOD calculation. Unlike the CMAQ RM method in which only AOEs from sulfate, nitrate, ammonium and sea salt have RH dependence, all the calculations for GOCART AOEs except hydrophobic BC/OC depend on ambient RH, wavelength and aerosol sizes, which differs from RM's one-size-fit-all method. It should be noted that the GSI AOD assimilation uses the 54 CMAQ species, not the GOCART species. The concentrations of the 54 species, aerosol sizes and ambient RH are feed into CRTM, which generates the AOD of each CMAQ species and the corresponding adjoint Jacobian, needed for the AOD assimilation (Figure 2). In GSI's AOD assimilation, the control variables are the 54 CMAQ aerosol species, unlike the GSI's $PM_{2.5}$ assimilation in which only $PM_{2.5}$ is the control variable and all CMAQ aerosol species are adjusted based on the $PM_{2.5}$ incremental ratio. In this study, GSI does not assimilate MODIS AOD and surface $PM_{2.5}$ simultaneously due to the

complexity of handling two observations types. For 18Z GSI assimilation, the assimilation was actually made in two steps: the first is the GSI AOD assimilation, and surface PM2.5 assimilation was made upon the AOD assimilation adjustment. After the assimilations, we get the adjusted CMAQ aerosol concentrations, which are used as the initial condition of the next cycle of the CMAQ forward run.

Figure 3 shows one example of the AOD calculations from the 3 methods mentioned above compared to Terra/Aqua MODIS AOD data. The MODIS AODs in Figure 3 are the daily data, and the overpass times of Terra and Aqua satellites on 07/01/2011 ranges from 15 to 22 UTC over the CONUS. Both OI and GSI use the AOD assimilation window of +/- 2 hours. During this event, some wildfire occurred in Southern Canada-Wisconsin, North and South Carolinas, which caused the relatively high AOD values. These high AODs are also confirmed by the MODIS retrievals (Figure 3d). Figure 3 shows that the different AOD calculations from the same CMAQ aerosol mass loadings yield the similar spatial distribution pattern with noticeable quantitative differences, and in general we see RM AOD > Mie AOD > CRTM AOD. In most regions, especially over Western USA, e.g. Nevada, MODIS AOD is higher than the three CMAQ AODs. The Mie-method AOD and CRTM AOD are generally lower than MODIS AOD. Only RM method shows some sporadic overestimated AOD over Southern Canada-Wisconsin and Carolinas. These differences will lead to the corresponding differences in data assimilation adjustments. Roy et al. (2007) compared the CMAQ AOEs with surface AOE observations from the nephelometer instrument over 25 Interagency Monitoring of Protected Visual Environment (IMPROVE) sites (most of them were located in National Parks), and found that the CMAQ RM method yielded too high surface AOE, but agreed well with AERONET (Aerosol Robotic Network) and MODIS AOD in summer 2001. In Roy et al. (2007), CMAQ used static lateral boundary condition, which may miss some elevated aerosol loadings (Lu et al., 2016). It is very likely that their CMAQ overpredicted near-surface AOD loading and underpredicted elevated AOD loading, but got total column AOD in right magnitude. In another word, the converting factors of RM method used in equation (3) may be too high if their CMAQ predicted correct aerosol mass concentration over those National Park sites.

2.3 $PM_{2.5}$ Calculations

Besides the MODIS AOD, The data assimilations of OI and GSI also use surface $PM_{2.5}$ observations to make adjustments. The OI method for surface $PM_{2.5}$ assimilation was described in Tang et al. (2015). Pagowski et al. (2014) described the GSI method for surface $PM_{2.5}$ assimilation used in WRF-CHEM in which aerosol size bins are fixed. CMAQ's $PM_{2.5}$ calculation is slightly different as it is not defined by fixed size bins, but three size modes: Aitken, accumulations and coarse modes (i, j, k modes) (Appel et al., 2010).

$$PM_{2.5} = PM25AT * (SO4_i + NO3_i + NH4_i + Na_i + Cl_i + EC_i + POC_i + OTHER_i) + PM25AC * (SO4_j + NO3_j + NH4_j + Na_j + Cl_j + EC_j + EL_j + POC_j + SOA_j + OTHER_j) + PM25CO * (SO4_k + NO3_k + NH4_k + Na_k + Cl_k + SOIL_k + OTHER_k) \quad (4)$$

where PM25AT, PM25AC and PM25CO are the mass scaling factors for the three modes, indicating the mass ratios of each mode falling in $PM_{2.5}$ size range (Jiang et al., 2006), and their value ranges should be between 0 and 1, varied with time and location. POC is the primary organic carbon, and SOA represents the 23 secondary organic aerosols (table 1). CMAQ 5.1 also includes 8 additional mineral elements: Fe, Al, Si, Ti, Ca, Mg, K and Mg (Table 1) in its accumulation mode, represented by EL_j. The species *OTHER* represent all other aerosols (Table 1) in each mode. The equation 4 describes the forward operator for calculating $PM_{2.5}$, which is feed into GSI as background $PM_{2.5}$ concentration. After the GSI estimates the total $PM_{2.5}$ increment, the increment is proportionally allocated to each aerosol size mode with the corresponding mass scaling factor, and then to each aerosol species. Thus, the final adjustment that OI and GSI give back to CMAQ is the mass concentration increment for each CMAQ aerosol species.

3. Results and Discussions

As the GSI and OI methods assimilate both surface $PM_{2.5}$ and AOD, the impacts of these adjustments can be compared. Figure 4 shows the CMAQ raw predictions (referred to as base-case run) of surface $PM_{2.5}$ compared to the measurements. In most regions west of 100ºW, this a priori case underestimated the surface $PM_{2.5}$. Surface measurement also shows some sporadic high $PM_{2.5}$ values in Eastern USA, missed by the base-case run. The goal of the data assimilations is to reduce these errors.

3.1 The Impact of Data Assimilation on Aerosol Mass Concentration

Since both $PM_{2.5}$ and aerosol AOD represent the concentrations of 54 aerosol species (Table 1), to understand the data assimilation method performances, we choose the accumulation-mode or J-mode sulfate (ASO4J), to illustrate the impact of data assimilation. Other aerosol species have similar adjustments in the GSI and OI assimilations. We set up three experiments to showing the assimilation effect, one with just PM2.5, one with AOD and one with both for the 18Z cycle. Figure 5 (a, b) shows that the GSI assimilation with surface $PM_{2.5}$ yields more significant changes than the corresponding OI assimilation. The OI assimilation of $PM_{2.5}$ leads to more localized increments compared to GSI since OI increment is spread over 11×11 grid cells (i.e., an area of 17424 km^2), while GSI increment spread depends on the horizontal length scales. Their adjustments also differ over certain areas. For instance, the base case underestimates $PM_{2.5}$ in Chicago, but it overestimates $PM_{2.5}$ in southeastern Wisconsin (Figure 4). The OI adjustment has a local flavor: increase ASO4J in Chicago, and decrease it over southeastern Wisconsin (Figure 5b). The GSI's result differs significantly due to its length scales and cost-function reduction over the whole domain. It yields overall $PM_{2.5}$ reduction in Chicago surrounding areas with smaller correction. Similar differences are also noted in other areas and other periods.

The impacts of AOD assimilations via GSI and OI also differ significantly (Figure 5c, 5d). The model relative uncertainty used in the OI assimilation is relatively high, which caused the strong

adjustment in ASO4J (Figure 5d) due to OI's AOD assimilation over Nevada-Southern California, Illinois and Michigan. The OI assimilation of AOD increases ASO4J over most of the model domain except in certain areas, such as Northeastern Minnesota-Southern Canada, and the eastern part of the border of North Carolina and South Carolina where the OI assimilation leads to a decrease in ASO4J (Figure 5d). The GSI assimilation of AOD tends to be more moderate and smoother. Its increment is almost one order of magnitude smaller than the variation of OI-AOD assimilation (Figure 5c). Figure 5c shows that the majority of increments of GSI-AOD assimilation occur in Eastern California-Nevada, Missouri-Illinois (St. Louis surrounding areas) and Wisconsin.

Figures 5e and 5f show the combined effect of assimilation of both surface $PM_{2.5}$ and AOD on surface ASO4J from GSI and OI methods, respectively. For GSI, the impact of assimilating surface $PM_{2.5}$ is greater than that of assimilating MODIS AOD. The OI assimilations show the opposite effect with AOD assimilation having a bigger impact than its surface $PM_{2.5}$ assimilation.

It should be noted that the difference between GSI and OI increments is not only on their horizontal distribution, but also on their vertical distribution. GSI has a height-dependent background error profile (Figure 1) while OI applies the uniform adjustment ratio to either whole column for AOD assimilation or below PBL for surface $PM_{2.5}$ assimilation. Figure 6 shows the model predicted PBL height at this time. In most portions of CONUS domain except the Rocky mountain region, the PBL height is less than 3 km. It means that the impact of OI-$PM_{2.5}$ assimilation should be below 3 km for most regions. Considering the locations of available surface $PM_{2.5}$ monitoring stations and the regional distribution of background $PM_{2.5}$, the vertical extension of the increments of OI-$PM_{2.5}$ should be more limited. Figure 7 shows the ASO4J increments similar to Figure 5 but for the model's 18^{th} layer, or roughly 2 km above ground. Figure 7b shows that the OI-$PM_{2.5}$ adjustment at the 2 km layer only appears in sporadic locations, such as Raleigh/Durham (central North Carolina), Atlanta and Denver downwind areas. Compared to Figure 5b and 6, we can find that in the most CONUS regions, the OI-$PM_{2.5}$'s ASO4J increments do not show up in the 2km layer because either their PBLs are lower than 2km, or there is no strong surface adjustment due to the locations of monitoring stations. On the contrary, GSI-$PM_{2.5}$ assimilation shows the horizontal distribution of ASO4J increment at 2km similar to its surface increment (Figure 7a, 5a), but with a much smaller magnitude than the increment of OI-$PM_{2.5}$ assimilation at the 2 km layer. The GSI-AOD assimilation also yields a similar ASO4J adjustment pattern with smaller increments than OI-AOD (Figure 7c, 5c). The strongest adjustment at the 2 km layer comes from the OI-AOD assimilation, which uses the same adjustment ratio for the whole vertical column. Its impact on 2 km ASO4J is more than one order of magnitude stronger than the corresponding GSI assimilation due to its relatively high uncertainty setting. In term of combined effect at the 2km, for GSI, the AOD assimilation is almost equally important as the surface $PM_{2.5}$ assimilation, depending on regions (Figure 7e).

For OI assimilation, the AOD's impact is dominated at the 2km layer as the surface $PM_{2.5}$'s effect only appear sporadically (Figure 7f).

3.2 The Impact of Data Assimilation on AODs

The above discussion is about the data assimilations' impacts on one aerosol mass concentration. It is also still needed to assess the impacts on column AODs, as the AOD is used here to make assimilations. Fortunately both CRTM and RM are composition-based methods for externally mixed aerosols, and we can easily calculate the AOD changes due to the changes of aerosol mass concentrations. Figure 8 shows the CRTM AOD changes due to GSI assimilation (left panel), and RM AOD changes due to OI assimilation (right panel). Their spatial distribution patterns are very similar to the corresponding surface ASO4J increments in Figure 5 as most high aerosol loadings are near surface. However, the AOD increment's value range of GSI-$PM_{2.5}$ assimilation is more than one order of magnitude lower than that of OI-$PM_{2.5}$. One reason is that the CRTM method yields 2 or 3 times lower AOD than the RM method with same aerosol loading (Figure 2b, 2c). Another reason, or the major reason, is that GSI-$PM_{2.5}$ assimilation has much lower increment on total aerosol mass loading, reflected by the magnitude difference between Figure 6a and 6b, as the GSI assimilation uses a steepen background error profile (Figure 1), makes its major adjustment near surface and yields smaller overall adjustment for total column aerosol mass loading. On the contrary, the OI-$PM_{2.5}$ assimilation applies the same adjustment ratio to the aerosol masses below PBL, and the adjustment could be much stronger than that of GSI-$PM_{2.5}$ assimilation for the elevated layers blow PBL. We can see the similar patterns and differences due to their AOD assimilations (Figure 8c, 8d). The AOD increments due to GSI-AOD and OI-AOD have the similar horizontal distribution to their corresponding ASO4J mass increments (Figure 5c,7c and 8c; Figure 5d, 7d, and 8d), but the OI-AOD has much stronger adjustments on total AOD and elevated aerosol masses. Generally, the GSI-AOD tends to increase AOD or aerosol column loading in Northern Central USA and over Nevada (Figure 8c). The OI-AOD assimilation has the similar AOD increment over these two regions, but decrease AOD or aerosol column loading over Texas, Northern Florida, South Central Canada, and the border of North Carolina and South Carolina (Figure 8d). It should be noted that the OI-$PM_{2.5}$ assimilation yields the AOD enhancements in Southern and Eastern USA, though just sporadically (Figure 8b). So there is a conflict as the OI-$PM_{2.5}$ and OI-AOD assimilations pointed to opposite adjusting directions over some areas, implying that the RM AOD could yield some overpredictions. Under this situation, the combined OI assimilations will increase below-PBL aerosol masses according to the adjustment of OI-$PM_{2.5}$, but reduce the above-PBL aerosol mass to fit the overall AOD reduction and get compromised results over these two regions (Figure 8f). This conflict-resolving process will change the vertical distribution of CMAQ aerosols. Figure 8 shows that the overall AOD increments are mainly due to $PM_{2.5}$ assimilation in GSI, and AOD assimilation in OI. The OI adjustments on AOD are much stronger than that of GSI, which is mainly due to their adjustments at the elevated layers.

3.3 The Overall Assimilation Impacts over Longer Periods

We continue the CMAQ runs after the 18UTC assimilations. After 1 hour, or at 19UTC, we compared their surface $PM_{2.5}$ prediction with the corresponding measurement again to see their impacts (Figure 9). At this time, the effects of data assimilations have been transported to downstream areas. Without the data assimilation, the base case (Figure 9a) systematically underestimated the $PM_{2.5}$ in western USA, which is consistent with that shown in Figure 4. Both assimilations correct some of the biases, which is more obvious in areas west of 90ºW. For instance, both assimilations correct the $PM_{2.5}$ underprediction in Iowa. In some locations, OI gets better result, such as in Southern Nevada-Southern Utah, and Kanas where only one surface observation is available. In other locations, the GSI achieves better results, such as Southeastern Wisconsin.Sometimes the data assimilations could overcorrect and yield worse results than the base run, such as the OI's overestimation over the Lake Michigan and GSI's overprediction over central Illinois (Figure 9b, 9c). The overcorrection issue is more evident in the OI run as the adjustment of the OI assimilation is stronger than that of GSI, due to OI's stronger setting for model uncertainties. This strong setting is actually helpful sometimes, for instance, the OI assimilation is strong enough to correct the underpredicting bias over southeastern North Carolina, where GSI's moderate correction only helps reduce that bias. The most evident side effect of the OI's overcorrection is the increase of root mean squared error (RMSE).

In this study, we employ 4-cycle per day data assimilations, the MODIS AOD assimilation is only applied at the cycle of 18 UTC for both the GSI and OI. We continue these runs for the whole July 2011, and make one-month continuous verification based on the 674 CONUS surface sites. In order to avoid from using the same data in data assimilation and verification, we skip verifying the initial condition of each 6-hour run. For 18UTC data assimilation and forecast, the verification starts from 19UTC to 00UTC, and 00UTC cycle's verification is made from 01UTC to 06UTC. The verification for rest cycles follows the similar time shift. Figure 10 shows the time-series plots of these CMAQ predictions for surface $PM_{2.5}$, their correlation coefficient (R) and RMSE. Before July 14 or Julian day 195, the CMAQ base prediction systemically underpredicted the PM2.5. After that date, the base model tends to underpredict during daytime, but slightly overpredict during nighttime, except for the last 3 days of July 2011 while the overall undeprediction appeared again. Both GSI and OI help reduce these undeprediction biases. The OI's correction is stronger due to its stronger setting. It became more evident during the $PM_{2.5}$ peak period caused by the firework emission at night of July 4^{th} (U.S. Independence Day), which is about early morning of July 5^{th} (Julian day 186) in UTC time (Figure 10a). The OI assimilation caught the firework caused PM2.5 spike though its peak time was later than that of the observation. The GSI assimilation showed the moderate correction which was not strong enough to full match with observation. The OI run shows some overprediction during the nighttime, especially in later July. Figure 10b clearly shows the effect of 4 assimilations per day, represented by the 4-time-per-day enhancement of GSI and OI's correlation coefficients. For the most of this month, we can generally see GSI>OI>CMAQ base for R. The difference of R between GSI and OI is much smaller than that between the assimilations runs and the CMAQ base case. GSI's R is consistent better than the CMAQ base while the OI's R is not always

better, e.g. during the Julian days of 191 and 207, though we can still find several periods when OI yielded the highest R. In term of RMSE, the GSI's RMSE is always lower than that of the base run, and the OI run shows some RMSE spikes (Figure 10c) due to its localized correction and strong settings.

Table 2 shows the corresponding statistics for the whole domain and the certain regions. The CMAQ base case systematically undepredicted surface $PM_{2.5}$ with mean bias of -2.25 $\mu g/m^3$ over CONUS during this period. With data assimilations, the OI and GSI runs get mean biases of 0.77 and -0.73 $\mu g/m^3$, respectively. Besides that effect, their correlation coefficient, R, is also improved: the base case's R is 0.3, and Rs of OI and GSI runs are 0.38 and 0.44 over CONUS, respectively. Their indexes of Agreement (IOA) have the corresponding improvements, too. Among the regions, the data assimilation yield most significantly improvements over the Pacific Coast and Southeastern USA, where the CMAQ base case has relatively poor correlation coefficients. In all of these regions, the GSI yields overall best correlation coefficient and RMSE, while the OI run has the smallest mean biases except for South Central region where the GSI's mean bias is the lowest. OI's localized correction and strong settings help get better mean biases, but cause the overcorrection issue and increase RMSE. Over Northeastern USA where relatively dense surface observations are available, the OI's RMSE increase is relatively small. Although both assimilations generally improve the $PM_{2.5}$ prediction, their performance can be highly varied depending on regions. For instance, over Rocky Mountain States where both surface observation and MODIS AOD are limitedly available with complex terrains, the GSI and OI assimilations slightly improve the R and IOA, though they evidently improve the mean bias of surface $PM_{2.5}$.

All these runs have daytime underprediction bias issue from 12 to 00UTC. The 4-cycle-per-day data assimilations help reduce that bias, but the bias trend is still there. It implies that the data assimilation for CMAQ's initial condition has certain limitation, and may not be able to solve the prediction bias by it alone. In addition to uncertainties in initial conditions, forecasts errors also depend on errors in model's meteorology, chemistry and emissions, and we need other adjustments to correct these biases.

4. Conclusions

In this study, we expanded the GSI assimilation to CMAQ 5.1's Aero6 aerosol species. The 4-cycle-per-day aerosol data assimilation for surface $PM_{2.5}$ and AOD were carried out with GSI and OI (Tang et al., 2015) methods over the CONUS. The results were compared against surface $PM_{2.5}$ observation, and shows that both assimilations generally improved the aerosol predictions. The increments resulting from our OI assimilation are spread in 11×11 horizontal grid cells while the increment spread in GSI (a 3D-Var assimilation technique) is controlled by its background error variances, horizontal and vertical length scales. GSI's cost function reduction is performed

for the whole domain. The differences in formulation of these two methods led to their different patterns of adjusting the initial conditions, and GSI yielded smoother and horizontally broader adjustment, but much weaker vertical increment. The local OI method uses a simple one-ratio-fit-all method for its vertical adjustment up to PBL height for $PM_{2.5}$ assimilation, or whole column for AOD assimilation. This OI method can use strong setting to achieve better mean bias, but has side effect of RMSE increase due to its localized correction. Overall, GSI's adjustment yield better results even with its moderate setting of data assimilation parameters, shown by its better statistics. One important reason is that GSI's whole-domain cost function reduction, which helps constrain its RMSE, and longer horizontal length scale, especially for $PM_{2.5}$ assimilation (Figure 1), which helps expand its adjusting effect to relatively broad areas. Both assimilations highly depend on the available observations. Compared to GSI's massive code, the OI code is much smaller and portable, which may be good choice of some light-duty usages.

AOD assimilations have more issues than the surface $PM_{2.5}$ assimilation, which is not only about the methods for converting aerosol mass concentrations to AOD that relies on the model for ambient RH, aerosol sizes and speciation, but also depends on a prior model for the aerosol vertical distribution. The CRTM AOD is about 2-3 times lower than RM AOD with the same aerosol mass loadings (Figure 3). From the existing evidence, the converting factors used in RM AOD may be too high (Roy et al., 2007), or the RM's one-size-fit-all method may not resolve highly-varied aerosol size impact on AOD calculation. There is another issue of aerosol specification, which is particular important for organic aerosols as CMAQ 5.1 has 23 SOAs plus primarily emitted OC (POC). All of organic aerosols were assumed to have the same optical properties in CRTM and RM, which is obviously an approximate assumption. Liu et al. (2016) shows that SOA's optical properties could be highly varied depending on the chemical species, aging time and ambient NOx concentrations. Both CRTM and RM assume that all aerosols are externally mixed, which may not best fit the situation in the real world. These uncertainties need to be addressed in the future verification with observations. In this study, we only adjust the aerosol mass concentrations, and did not adjust the aerosol composition, size and vertical distributions which could have big impact on the AOD calculations. The data assimilation for initial condition also has its limitation, and its adjustment effect could fade away with time if there is persistent model bias. So, more frequent adjustment is helpful. Unfortunately the MODIS AOD assimilation used in this study is applied only once per day in the data assimilations due to the data availability. More satellite AOD data, such as VIIRS (Visible Infrared Imaging Radiometer Suite) and GOES-R (Geostationary Operational Environmental Satellite-R Series) ABT (Advanced Baseline Imager) AODs, should make this assimilation more useful. Another approach is using more complex and costly four-dimensional (4-D) variational data assimilation (4D-var) to correct the model's persistent biases, which integrated the data assimilation with the CTM (Chai et al., 2016). All these issue should be addressed in the future studies.

Code Availability

This study includes the forward simulations and data assimilation tools. The meteorological code of WRF 3.4.1 can be downloaded from http://www2.mmm.ucar.edu/wrf/users/download/get_source.html. CMAQ 5.1 can be downloaded from https://www.cmascenter.org/download.cfm. The GSI data assimilation tool can be downloaded at http://www.dtcenter.org/com-GSI/users.v3.5/downloads/index.php. All other codes and the modified codes can be provided upon request.

Reference:

Adhikary, B., S. Kulkarni, A. Dallura, Y. Tang, T. Chai, L. R. Leung, Y. Qian, C. E. Chung, V. Ramanathan, and G. R. Carmichael. A regional scale chemical transport modeling of Asian aerosols with data assimilation of AOD observations using optimal interpolation technique. Atmos. Environ., 42(37). 8600-8615, 2008.

Appel, K. W., S. J. Roselle, R. C. Gilliam, and J. E. Pleim, Sensitivity of the Community Multiscale Air Quality (CMAQ) model v4. 7 results for the eastern United States to MM5 and WRF meteorological drivers. Geosci. Model Dev., 3, 169–188, 2010.

Binkowski, F. S., and S. J. Roselle, Models-3 Community Multiscale Air Quality (CMAQ) model aerosol component: 1. Model description, J. Geophys. Res., 108(D6), 4183, doi:10.1029/2001JD001409, 2003.

Bocquet M., Elbern H., Eskes H., Hirtl M., Žabkar R., Carmichael G. R., Flemming J., Inness A., Pagowski M., Pérez Camaño J. L., Saide P. E.: Data assimilation in atmospheric chemistry models: current status and future prospects for coupled chemistry meteorology models. Atmospheric chemistry and physics;15(10):5325-58, 2015

Chai T., H.C. Kim, L. Pan, P. Lee, and D. Tong, , Impact of Moderate Resolution Imaging Spectroradiometer (MODIS) aerosol optical depth (AOD) and AirNow PM2.5 assimilation on Community Multi-scale Air Quality (CMAQ) aerosol predictions over the contiguous United States, J. Geophys. Res., 122, doi:10.1002/2016JD026295.., 111, D02301, doi:10.1029/2006JD007763, 2006, 2017.

Chin, M., Rood, R. B., Lin, S.-J., Muller, J.-F., and Thompson, A. M.: Atmospheric sulfur cycle simulated in the global model GOCART: Model description and global properties, J. Geophys. Res., 105, 24671–24687, doi:10.1029/2000JD900384, 2000.

Chin, M., Ginoux, P., Kinne, S., Torres, O., Holben, B. N., Duncan, B. N., Martin, R. V. , Logan, J. A., and Higurashi, A.: Tropospheric aerosol optical thickness from the GOCART model and comparisons with satellite and Sun photometer measurements, J. Atmos. Sci., 59, 461–483, 2002.

Descombes, G., Auligné, T., Vandenberghe, F., Barker, D.M. and Barre, J., Generalized background error covariance matrix model (GEN_BE v2. 0). Geoscientific Model Development, 8(3), pp.669-696, doi:10.5194/gmd-8-669-2015, 2015.

Elbern, H. and Schmidt, H.: A 4D-Var chemistry data assimilation scheme for Eulerian chemistry transport modelling, J. Geophys. Res., 104, 18583–18598, 1999.

Elbern, H. and Schmidt, H.: Ozone episode analysis by four dimensional variational chemistry data assimilation, J. Geophys. Res., 106, 3569–3590, 2001.

Elbern, H., Schmidt, H., and Ebel, A.: Variational data assimilation for tropospheric chemistry modelling, J. Geophys. Res., 102, 15967–15985, 1997.

Elbern, H., Schmidt, H., Talagrand, O., and Ebel, A.: 4D-variational data assimilation with an adjoint air quality model for emission analysis, Environ, Model. Softw., 15, 539–548, 2000.

Elbern, H., Strunk, A., Schmidt, H., and Talagrand, O.: Emission rate and chemical state estimation by 4-dimensional variational inversion, Atmos. Chem. Phys., 7, 3749–3769, doi:10.5194/acp-7-3749-2007, 2007.

Han, Y., van Delst, P., Liu, Q., Weng, F., Yan, B., Treadon, R., and Derber, J.: JCSDA Community Radiative Transfer Model (CRTM) – Version 1, NOAA Tech. Rep. NESDIS 122, 33 pp., NOAA, Silver Spring, Md, 2006.

Jiang, W., Smyth, S., Giroux, E., Roth, H., and Yin, D.: Differences between CMAQ fine mode particle and $PM_{2.5}$ concentrations and their impact on model performance evaluation in the lower Fraser valley, Atmos. Environ., 40, 4973–4985, 2006

Lee P, McQueen J, Stajner I, Huang J, Pan L, Tong D, Kim H, Tang Y, Kondragunta S, Ruminski M, Lu S. NAQFC developmental forecast guidance for fine particulate matter (PM2. 5). Weather and Forecasting, 32(1):343-60, 2017.

Levy, R. C., L. A. Remer, D. Tanré, S. M attoo, and Y. J. K aufman, Algorithm for remote sensing of tropospheric aerosol over dark targetsfrom MODIS: Collections 005 and 051, NASA Goddard Space Flight Center, Greenbelt, Md. [Available at http://modis-atmos.gsfc.nasa.gov/_docs/ATBD_MOD04_C005_rev2.pdf, revision2.], 2009.

Liu, J., P. Lin, A. Laskin, J. Laskin, S. M. Kathmann, M. Wise, R. Caylor, F. Imholt, V. Selimovic and J. E. Shilling, Optical properties and aging of light-absorbing secondary organic aerosol, Atmos. Chem. Phys., 16, 12815–12827, doi:10.5194/acp-16-12815-2016, 2016.

Liu, Z., Liu, Q., Lin, H.-C., Schwartz, C. S., Lee, Y.-H., and Wang, T.: Three-dimensional variational assimilation of MODIS aerosol optical depth: Implementation and application to a dust storm over East Asia, J. Geophys. Res., 116, D22306, doi:10.1029/2011JD016159, 2011.

Liu, Q. and Weng, F.: Advanced doubling-adding method for radiative transfer in planetary atmospheres, J. Atmos. Sci., 63, 3459–3465, 2006.

Lu, C.-H., A. da Silva, J. Wang, S. Moorthi, M. Chin, P. Colarco, Y. Tang, P. S. Bhattacharjee, S.-P. Chen, H.-Y. Chuang, H.-M. H. Juang, J. McQueen, and M. Iredell, The implementation of NEMS GFS Aerosol Component (NGAC) Version 1.0 for global dust forecasting at NOAA/NCEP, Geosci. Model Dev., 9, 1905-1919, doi:10.5194/gmd-9-1905-2016, 2016.

Malm, W. C., J. F. Sisler, D. Huffman, R. A. Eldred, and T. A. Cahill, Spatial and seasonal trends in particle concentration and optical extinction in the United States, J. Geophys. Res., 99, 1347–1370, 1994.

Pagowski, M., Z. Liu, G. A. Grell, M. Hu, H.-C. Lin, C. S. Schwartz: Implementation of aerosol assimilation in Gridpoint Statistical Interpolation (v. 3.2) and WRF-Chem (v. 3.4.1), Geosci. Model Dev., 7, 1621–1627, doi:10.5194/gmd-7-1621-2014., 2014.

Pan, L., D.Q. Tong, P. Lee, H. Kim and T. Chai, Assessment of NOx and O3 forecasting performances in the U.S. National Air Quality Forecasting Capability before and after the 2012 major emissions updates, Atmospheric Environment, 95, 610-619. doi:10.1016/j.atmosenv.2014.06.020, 2014.

Parrish D. F. and Derber J. C.: The National Meteorological Center spectral statistical interpolation analysis system, Mon. Weather Rev., 120, 1747–1763, 1992.

Purser, R. J., Wu, W.-S., Parrish, A. F., and Roberts, N. M.: Numerical aspects of the application of recursive filters to variational statistical analysis. Part I: Spatially homogeneous Gaussian covariances, Mon. Weather Rev., 131, 1524–1535, 2003a.

Purser, R. J., Wu, W.-S., Parrish, A. F., and Roberts, N. M.: Numerical aspects of the application of recursive filters to variational statistical analysis. Part II: Spatially inhomogeneous and anisotropic general covariances, Mon. Weather Rev., 131, 1536–1549, 2003b.

Remer, L.A., Kaufman, Y.J., Tanré, D., Mattoo, S., Chu, D.A., Martins, J.V., Li, R.R., Ichoku, C., Levy, R.C., Kleidman, R.G. and Eck, T.F.. The MODIS aerosol algorithm, products, and validation. *J. Atmos. Sci.*, 62(4), pp.947-973, 2005.

Roy, B., R. Mathur, A. B. Gilliland, and S. C. Howard, A comparison of CMAQ-based aerosol properties with IMPROVE, MODIS, and AERONET data, J. Geophys. Res., 112, D14301, doi:10.1029/2006JD008085, 2007.

Sonntag, D. B., R. W. Baldauf, C. A. Yanca and C. R. Fulper, Particulate matter speciation profiles for light-duty gasoline vehicles in the United States, Journal of the Air & Waste Management Association, 64:5, 529-545, DOI:10.1080/10962247.2013.870096, 2014.

Tang, Y., T. Chai, L. Pan, P. Lee, Daniel Tong, H. Kim, and W. Chen, Using Optimal Interpolation to Assimilate Surface Measurements and Satellite AOD for Ozone and $PM_{2.5}$: A Case Study for July 2011. Journal of the Air & Waste Management Association, DOI:10.1080/10962247.2015.1062439, 2015.

Tang, Y., P. Lee, M. Tsidulko, H.-C. Huang, J. T. McQueen, G. J. DiMego, L. K. Emmons, R. B. Pierce, A. M. Thompson, H.-M. Lin, D. Kang, D. Tong, S.-C. Yu, R. Mathur, J. E. Pleim, T. L. Otte, G. Pouliot, J. O. Young, K. L. Schere, P. M. Davidson and I. Stajner, The Impact of

chemical lateral boundary conditions on CMAQ predictions of tropospheric ozone over the Continental United States, Environmental Fluid Mechanics, doi:10.1007/s10652-008-9092-5, 2008.

Whitby, E. R., and P. H. McMurry, Modal aerosol dynamics modeling. Aerosol Science and Technology 27: 673-688, 1997.

Wu, W.-S., Purser, R. J., and Parrish, D. F.: Three-dimensional variational analysis with spatially inhomogeneous covariances, Mon. Weather Rev., 130, 2905–2916, 2002.

Table 1. CMAQ 5.1 aerosol species and their Mapping to GOCART aerosol optical properties in CRTM. (CMAQ species with solid underline are Aitken-mode aerosols, and those with dash underline are coarse-mode aerosols, and the rest are the accumulation-mode aerosols)

Aerosol Species in CMAQ 5.1	**GOCART aerosols in CRTM**
ASO4I ANO3I ANH4I ACLI ASO4J ANO3J ANH4J ASO4K ANO3K ANH4K	Sulfate Aerosol
AECI AECJ	Black Carbon Aerosol
APOCI APNCOMI APOCJ AOTHRJ AXYL1J AXYL2J AXYL3J ATOL1J ATOL2J ATOL3J ABNZ1J ABNZ2J ABNZ3J AISO1J AISO2J AISO3J ATRP1J ATRP2J ASQTJ AALK1J AALK2J AORGCJ AOLGBJ AOLGAJ APAH1J APAH2J APAH3J APNCOMJ	Organic Carbon Aerosol
AFEJ AALJ ASIJ ACAJ AMGJ AKJ AMNJ ACORS ASOIL	Dust Aerosol
ANAJ ACLJ ACLK ASEACAT	Sea Salt Aerosol

Table 2. Regional statistic of the three simulations (CMAQ_BASE, OI and GSI) for surface $PM_{2.5}$ in July, 2011

Regions	Simulations	Mean Bias ($\mu g/m^3$)	Root Mean Square Error ($\mu g/m^3$)	Correlation Coefficient, R	Index of Agreement
CONUS	BASE	-2.25	10.57	0.3	0.54
	OI	0.77	11.07	0.38	0.59
	GSI	-0.73	9.42	0.44	0.64
Northeastern USA	BASE	-3.36	11.02	0.27	0.54
	OI	0.78	11.17	0.42	0.64
	GSI	-1.18	9.70	0.44	0.66
Pacific Coast	BASE	-2.24	8.74	0.23	0.40
	OI	0.71	9.13	0.40	0.60
	GSI	-0.80	7.86	0.44	0.61
Southeastern USA	BASE	-1.86	11.05	0.23	0.50
	OI	0.12	9.88	0.41	0.63
	GSI	-0.58	9.30	0.41	0.63
Rocky Mountain States	BASE	-3.22	12.14	0.09	0.24
	OI	1.59	13.28	0.13	0.30
	GSI	-1.63	11.75	0.16	0.28
North Central	BASE	-1.55	12.29	0.22	0.49
	OI	0.96	13.83	0.28	0.51
	GSI	-0.26	11.12	0.35	0.59
South Central	BASE	-1.1	9.49	0.09	0.4
	OI	0.38	8.07	0.27	0.52
	GSI	-0.1	7.58	0.27	0.54

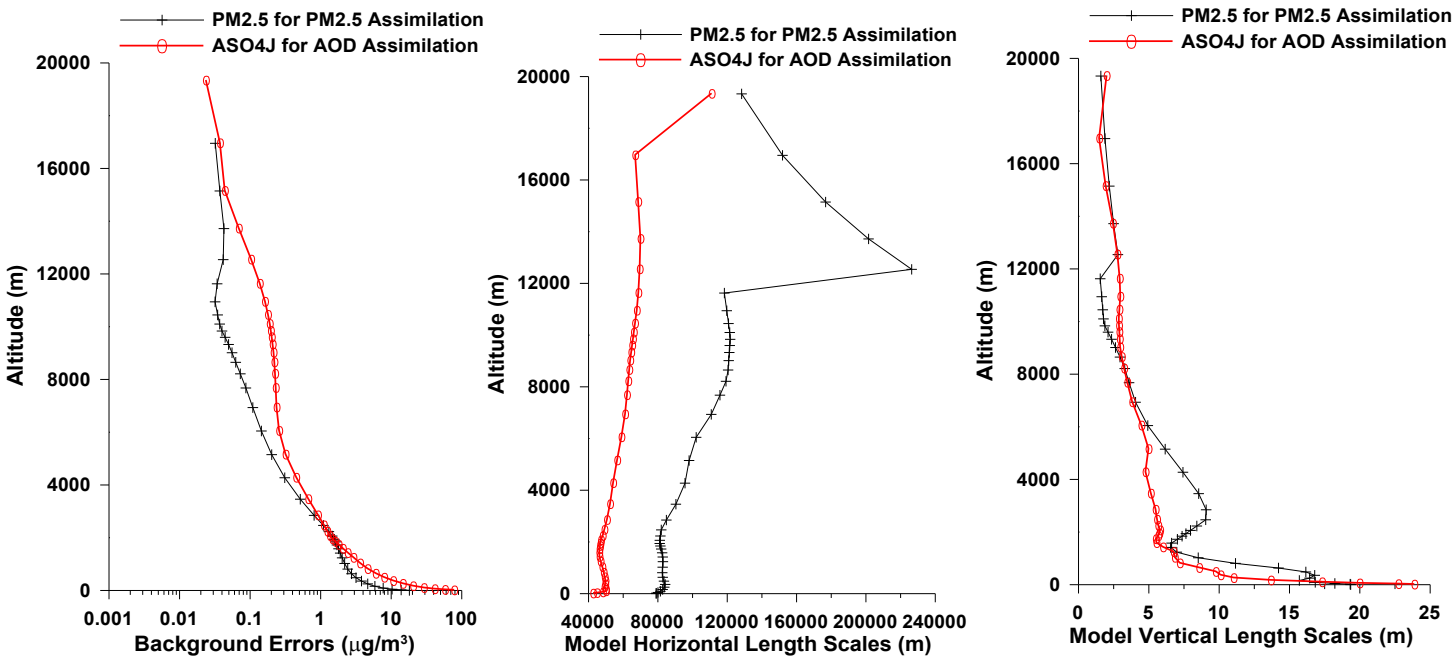

Figure 1. GSI's background errors and length scales used in this study (ASO4J is the CMAQ's accumulation-mode sulfate aerosol)

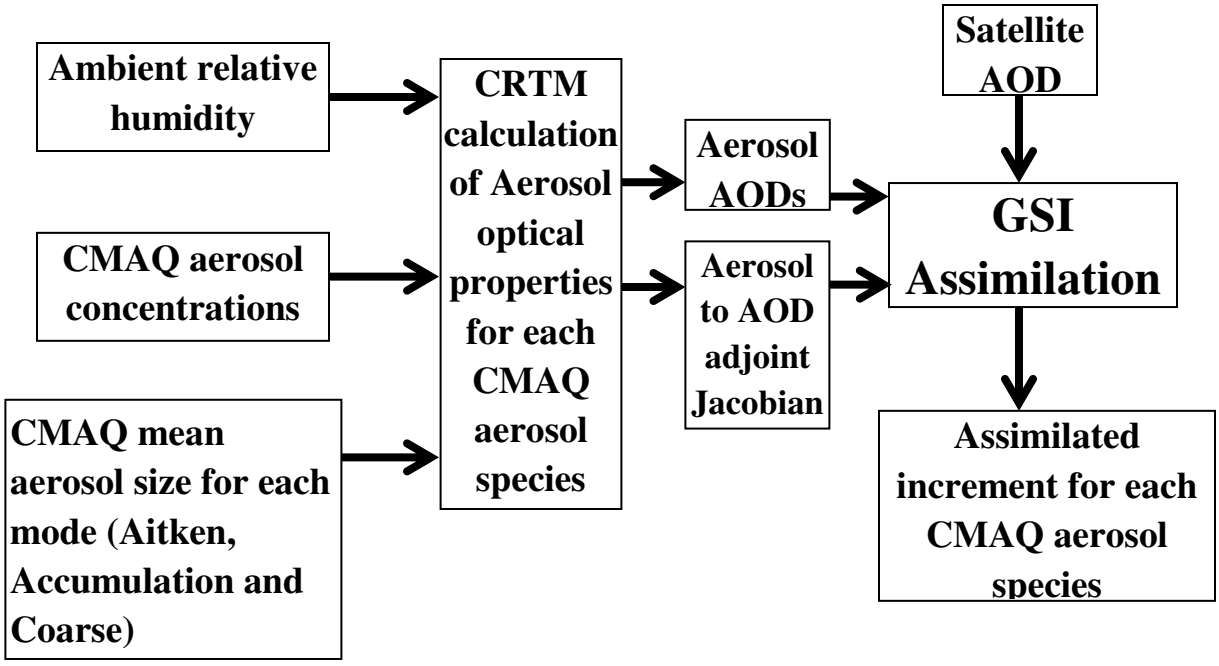

Figure 2. The schematic diagram of GSI-AOD assimilation

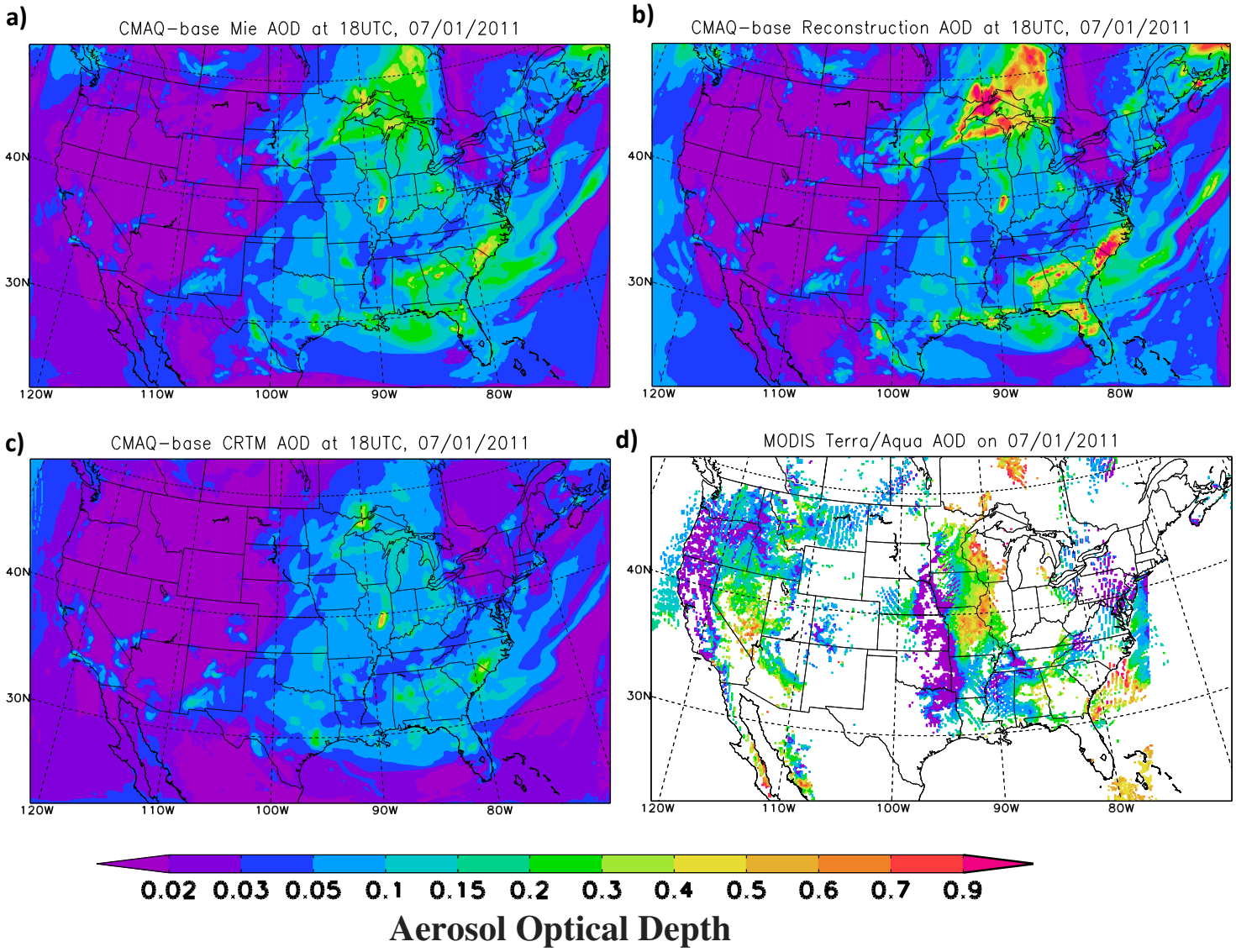

Figure 3, AOD calculations using Mie-method (a), reconstruction method (b), and CRTM from the CMAQ's base case (before assimilations) compared to MODIS AOD on 07/01/2011. All the AODs are at 550nm wavelength.

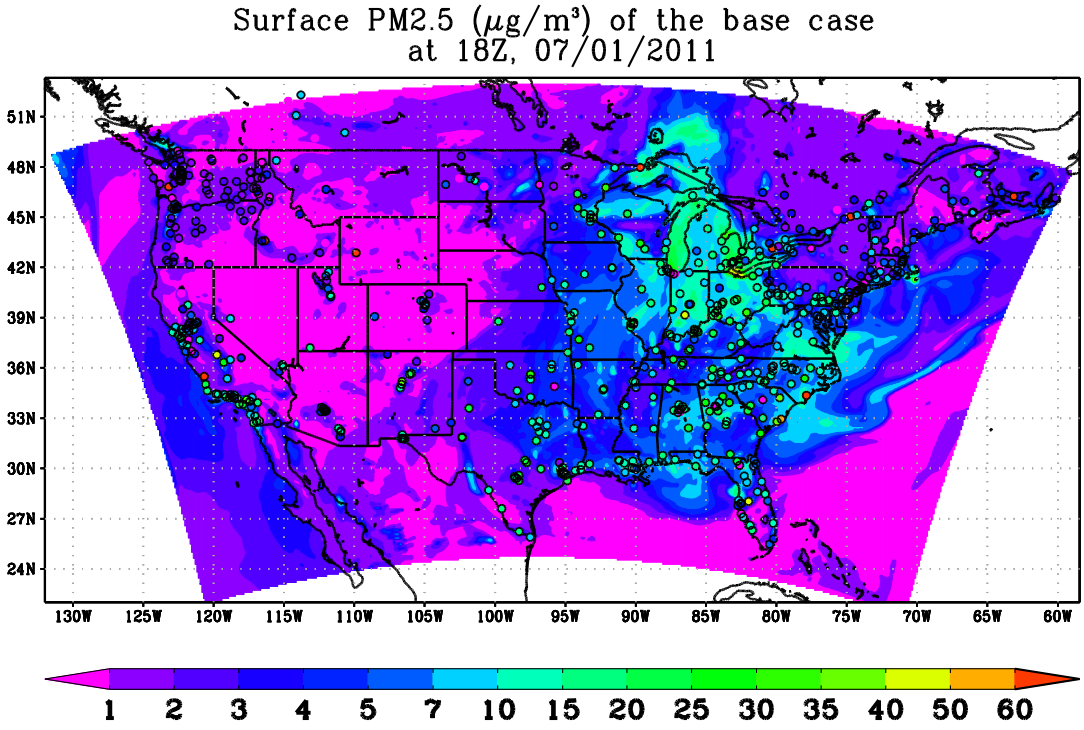

Figure 4. Predicted surface $PM_{2.5}$ from CMAQ base run compared to surface measurement (close circle) at 18 UTC, 07/01/2011.

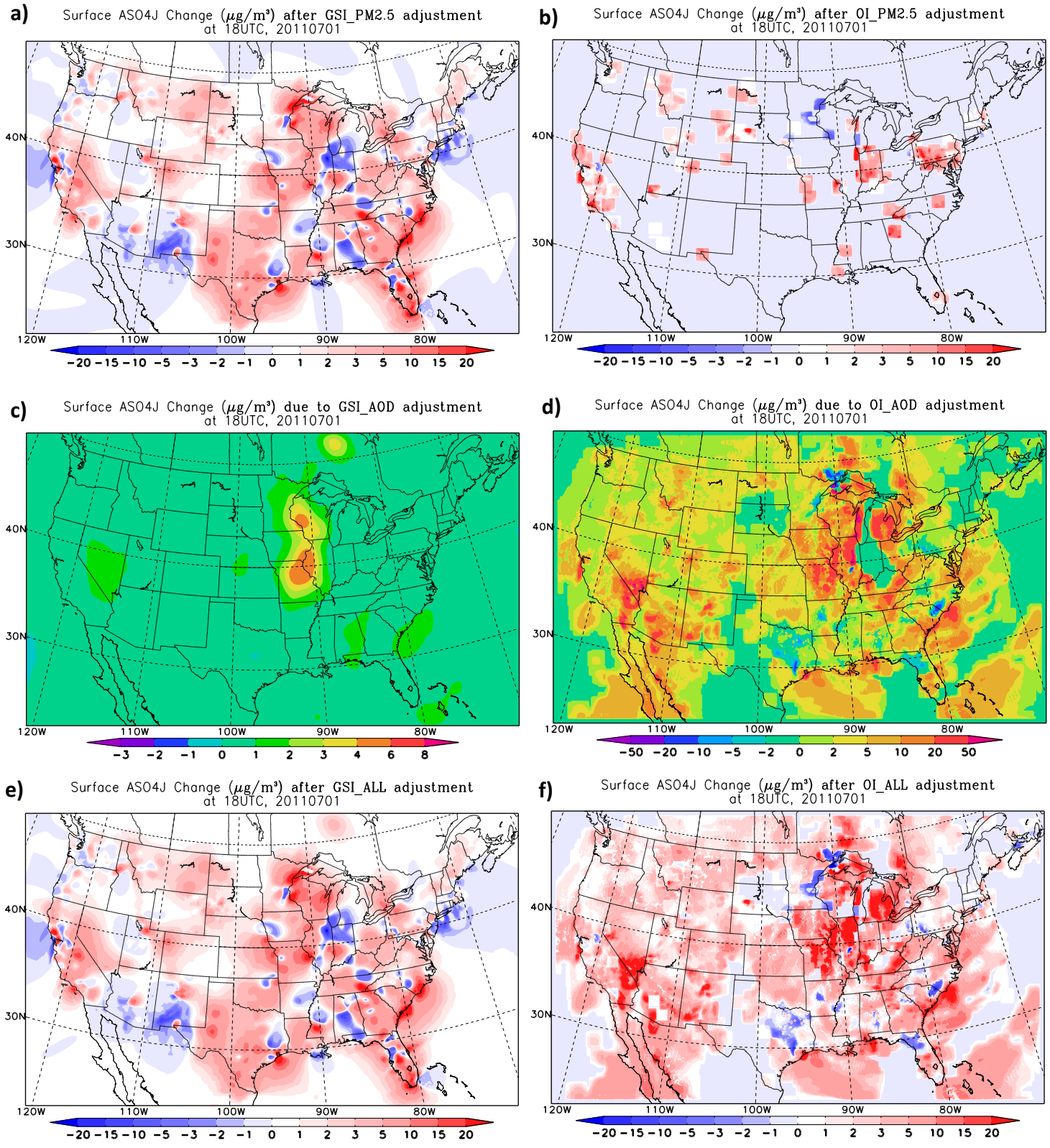

Figure 5. surface accumulation-mode sulfate (ASO4J) changes after GSI (left) and OI (right) assimilations with surface $PM_{2.5}$ and MODIS AOD at 550nm.

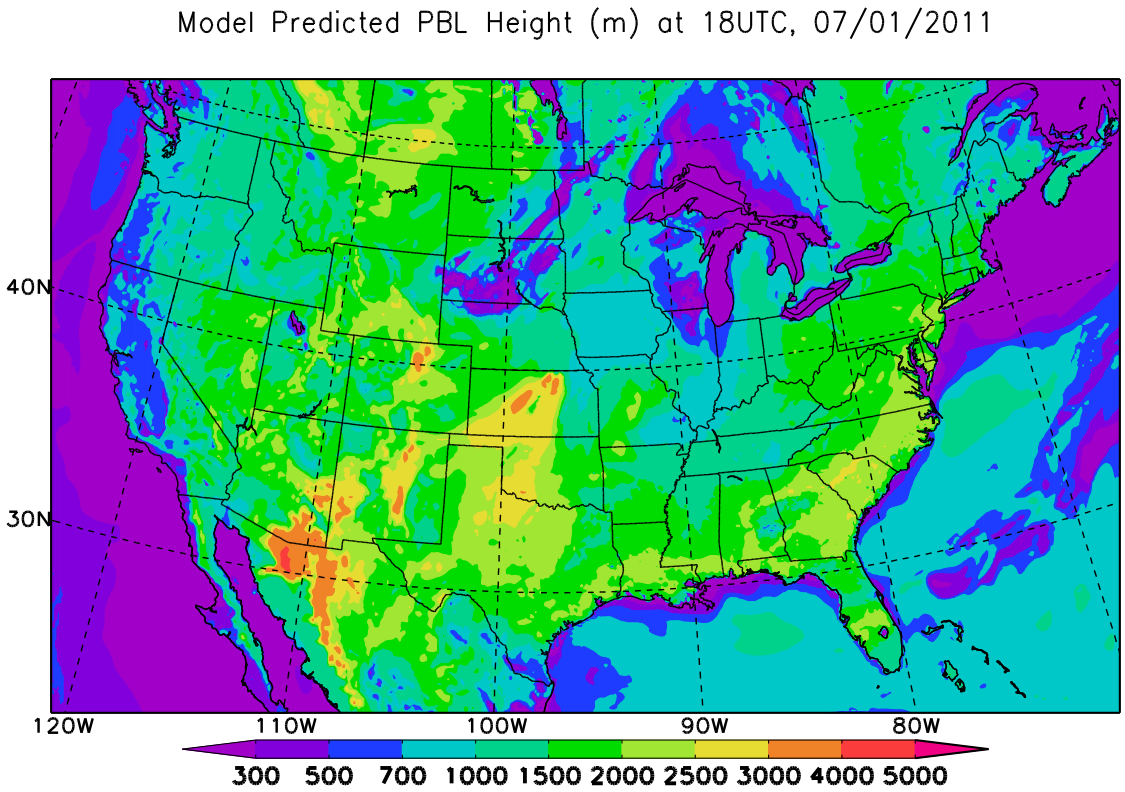

Figure 6. Model-Predicted PBL height (m) at 18UTC, 07/01/2011

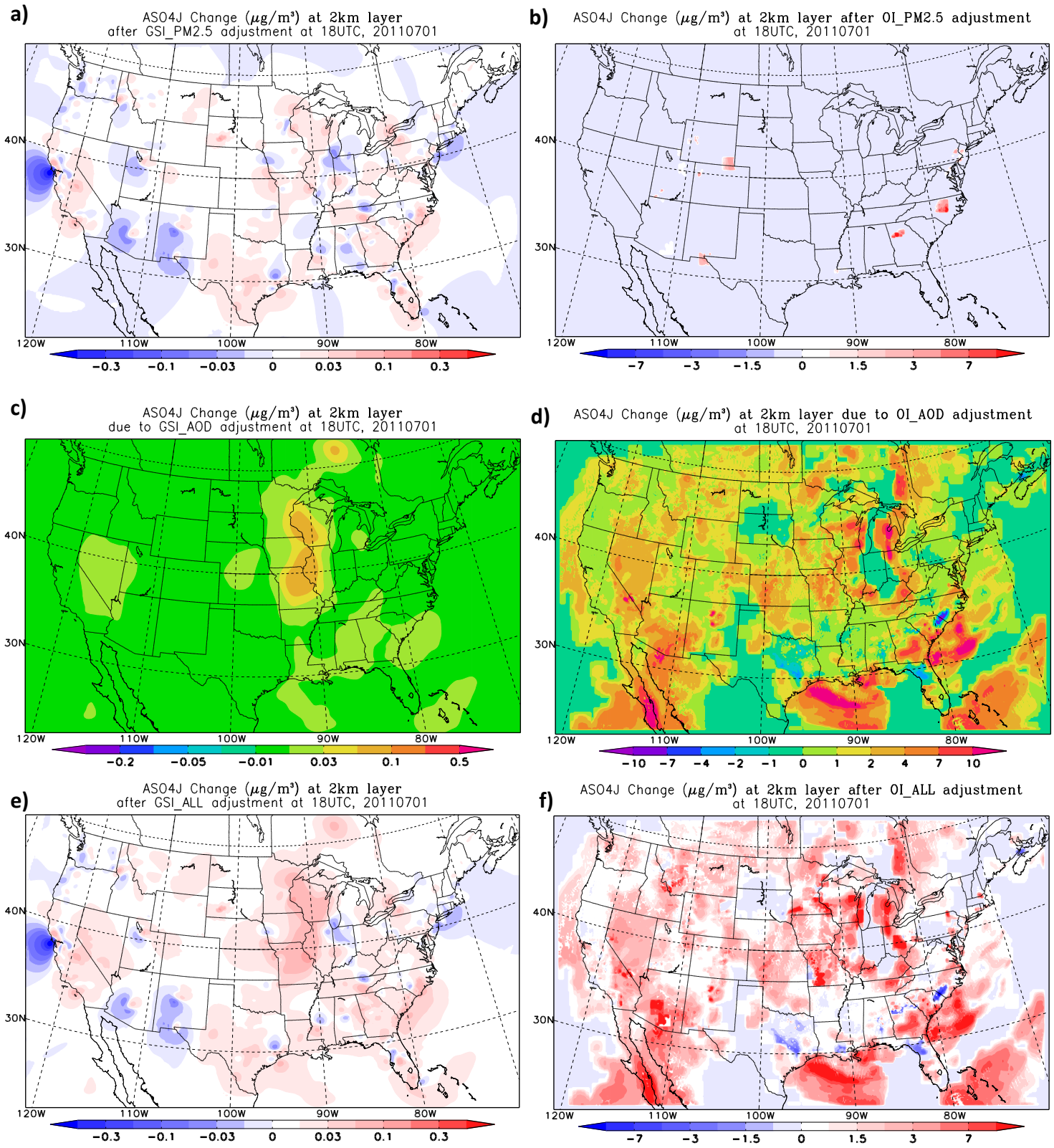

Figure 7, same as the figure 5 but for the model's 2km layer.

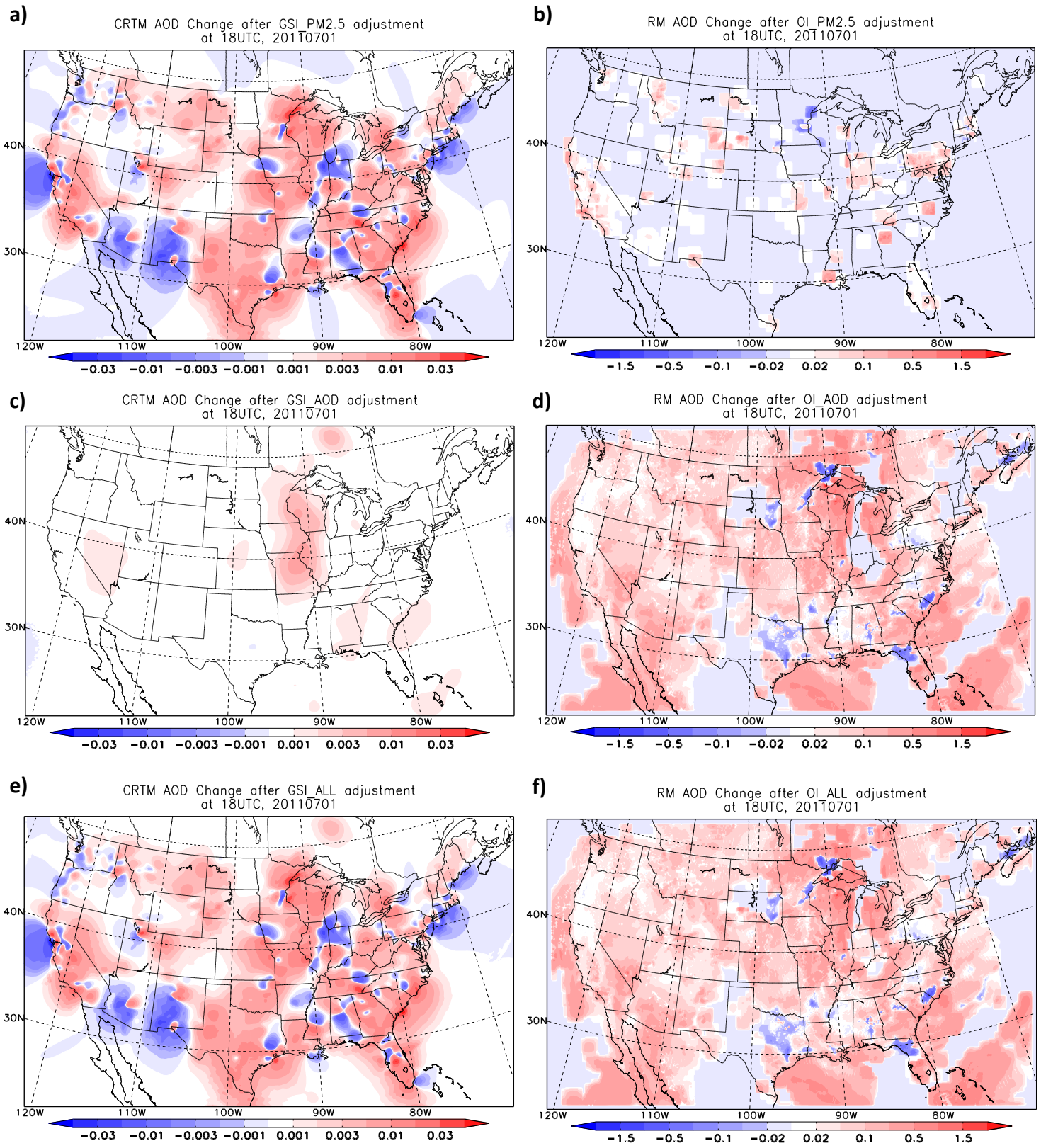

Figure 8, same as the Figure 5 but for AOD (at 550nm) change. Left plots show the CRTM AOD change due to GSI adjustments and right plots are RM AOD change for OI.

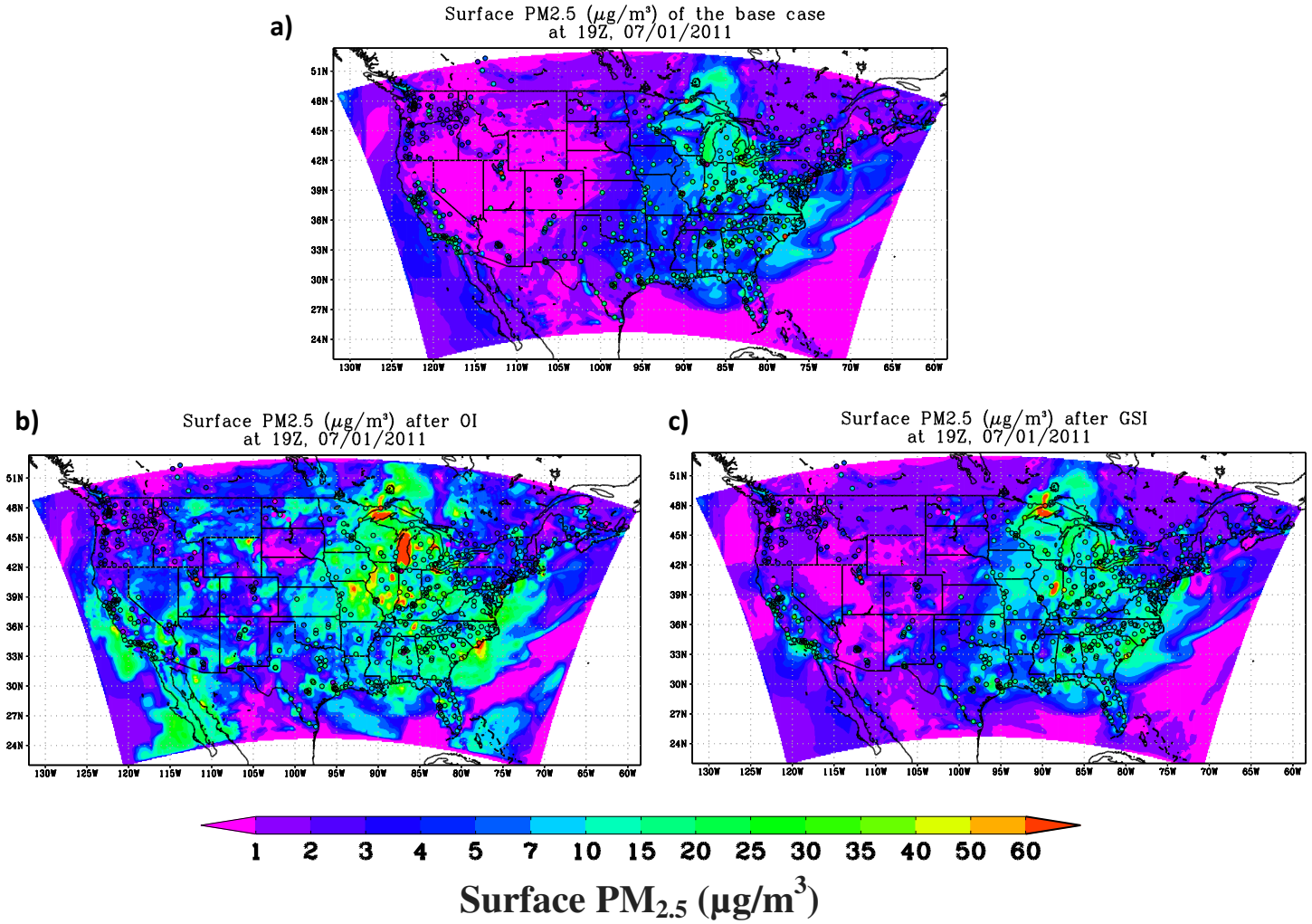

Figure 9, Predicted surface $PM_{2.5}$ from the base case (a), OI (b) and GSI (c) runs compared to surface observation at 19UTC, 07/01/2011.

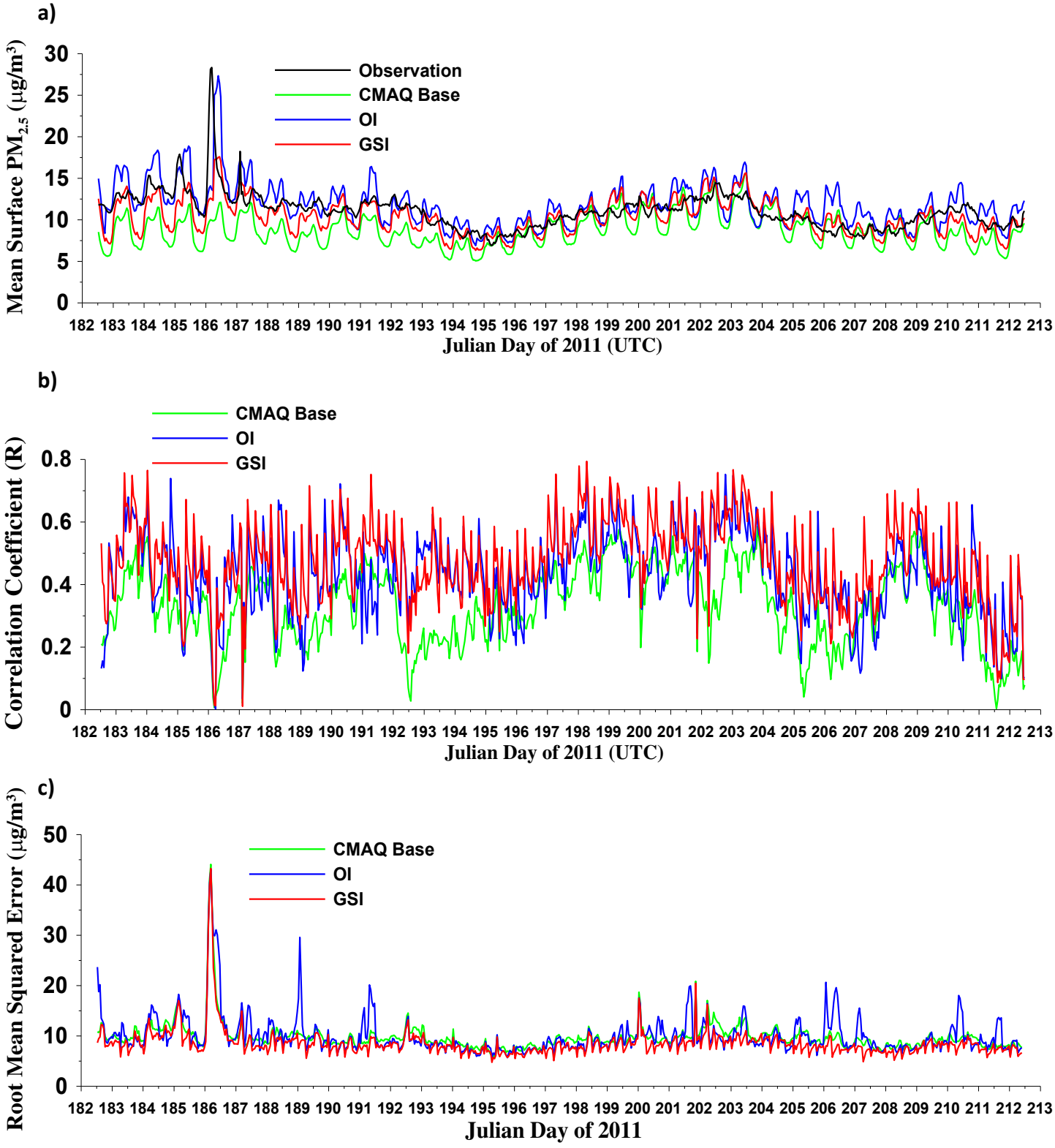

Figure 10, Time-series comparisons of CMAQ surface $PM_{2.5}$ (base, OI, and GSI) versus the observation over the CONUS domain for their mean value (a), correlation coefficient (b) and root mean squared error (RMSE) (c)